Investigation of Wideband Multi-Element Multi-Segment Half-Sectored Cylindrical Dielectric Resonator Antenna for Wireless Applications

Pinku Ranjan[1, *] and Ravi K. Gangwar[2]

Abstract—This paper presents the design and development of a multi-element multi-segment half-sectored Cylindrical Dielectric Resonator Antenna (MEMS h-CDRA) with coaxial probe feed. The input and radiation characteristics of the proposed MEMS h-CDRA are investigated through the Ansoft HFSS simulation software. To validate the antenna performance, the proposed h-CDRA is fabricated and experimentally investigated. The simulation results are compared with measured data, and they are in good agreement with each other. The proposed MEMS h-CDRA is excited with coaxial probe feed, which excites $TM_{01\delta}$ dominant mode fields in the h-CDRA elements. The proposed MEMS h-CDRA provides wide bandwidth ($\approx 120.3\%$) with gain of 6.45 dBi at resonant frequency (6.4 GHz). The measured gain is more than 4.0 dBi in entire operating frequency band (5.3 GHz–13.0 GHz) with monopole type radiation pattern. The bandwidth as well as gain enhancement is experimentally observed in the proposed structure. The proposed antenna has found suitable application for WLAN and WiMAX as well as X-band wireless applications.

1. INTRODUCTION

In last two decades, wideband antenna has been investigated for wireless communication. Unlike a conventional microstrip antenna, Dielectric Resonator Antenna (DRA) offers several advantages such as zero conductor losses due to absence of surface wave, high radiation efficiency, light weight, small size, and ease of excitation, which is suitable for wireless applications [1, 2]. Once Dielectric Resonators (DRs) are left in open environment, it radiates like an antenna. Low loss dielectric material ($\tan \delta \approx 10^{-4}$) has been used for fabrication of DRAs. Cylindrical dielectric resonator has been investigated by Long et al. as an efficient radiator [3]. The radiation characteristic of cylindrical DRA depends upon mode of excitation. It has been excited with some fundamental modes such as $TE_{01\delta}$, $TM_{01\delta}$, $HE_{11\delta}$, $EH_{11\delta}$, and $TE_{011+\delta}$ [4].

For bandwidth enhancement, experimentally broadband DRA was first investigated by Kishk et al. in 1989 with stacking of DRA over one on another [5]. Since then, several techniques have been explored by many researchers for bandwidth enhancement. Various methods include stacking/multi-segments [5–8], changing the aspect ratio of DRA [9], multi-element concept [10], sectoring/splitting of the basic structure [11–14], and an air gap introduction below the DRA [15–17]. Using multi-segment technique, wideband performance has been achieved by Petosa et al. for a rectangular DRA, in which low dielectric material has been inserted below the DRA [6]. Stacking of the annular ring DRA with coaxial probe feed has been investigated for improvement in bandwidth by Luk et al. [7]. The triangular DRA has also been investigated with segmentation approach for bandwidth enhancement and found to have 35% bandwidth [8].

* Corresponding author: Pinku Ranjan (pinkuranjan@iiitm.ac.in).

[1] Atal Bihari Vajpayee-Indian Institute of Information Technology and Management (ABV-IIITM), Gwalior-474015, India.
[2] Department of Electronics Engineering, Indian Institute of Technology (Indian School of Mines), Dhanbad, India.

Through the splitting/sectoring of DRA, bandwidth can also be enhanced. It has one advantage that the effective volume of the DRA will be unchanged. The splitting of the basic cylindrical shape has been proposed by Mongia et al. for bandwidth enhancement with monopole type radiation pattern of the DRA [11, 12]. Through compact cylindrical sector DRA, 75% volume can be reduced as compared to a conventional cylindrical DRA with same antenna performance [13]. A half split hemispherical DRA has been investigated for low profile monopole type DRA as broadband variants with 35% bandwidth enhancement in [14].

Monopole type radiation pattern has been presented by several researchers for different DRA shapes [18–22]. The first DRA based article has been reported by Mongia et al. for generation of monopole type radiation pattern [18]. For $TM_{01\delta}$ mode excitation, the circle-shaped dielectric ring resonator has been excited by coaxial probe feed. The monopole like radiation pattern has also been demonstrated by Guha and Antar for a four elements CDRA which shows nearly 29% impedance bandwidth [10]. Multi-element technique has been investigated for different DRA shapes for bandwidth enhancement such as four elements rectangular and triangular DRAs, which provide nearly 35% bandwidth with monopole type radiation pattern [21, 22, 28]. The monopole type radiation has also been achieved through splitting/sectoring of cylindrical DRA [24–26, 29, 30].

In this paper, a cylindrical DRA is investigated with geometrical modification i.e., split/sector of cylindrical shape in two uniform parts and named as half split cylindrical DRA (h-CDRA). Further, multi-segment technique is applied on both h-CDRAs and fed through a co-axial probe at the center. $TM_{01\delta}$ has been excited through this feeding approach. The proposed antenna provides wide bandwidth with good gain. The design and development of MEMS h-CDRA are performed through Ansoft HFSS simulation software. The proposed prototype is fabricated. The simulated antenna performance is verified experimentally through measurement. The proposed MEMS h-CDRA provides 120.3% bandwidth ($|S_{11}| \leq -10$ dB) and 6.45 dBi gain at 6.4 GHz resonant frequency. The proposed antenna provides a uniform monopole-like radiation pattern over the complete operating frequency band.

2. ANTENNA DESIGN AND ANALYSIS

The cylindrical DRA has been sectored from a mold cylinder with a certain angle, which is shown in Fig. 1. The arbitrary angle (β) is proposed to split a cylinder in uniform part. The sectored cylindrical DRA is kept on a ground plane. The sectored cylindrical DRA face is left open. Due to air exposed sectored face, approximately magnetic wall boundary conditions can be applied. Through a magnetic wall approximation for a complete sectored surface, fields inside the cylindrical sector DRA in terms of TM_{mnp} modes are [3]

$$E_z^{mnp} = [AJ_m (k_r r) + BY_m (k_r r)] \cdot [C \sin (v\emptyset) + D \cos (v\emptyset)] \cos (k_z z) \tag{1}$$

Here A, B, C, and D are arbitrary constants. These arbitrary constants depend upon location and type of feed of the DRA, whereas J_m and Y_m denote the first and second kinds of mth-order Bessel function,
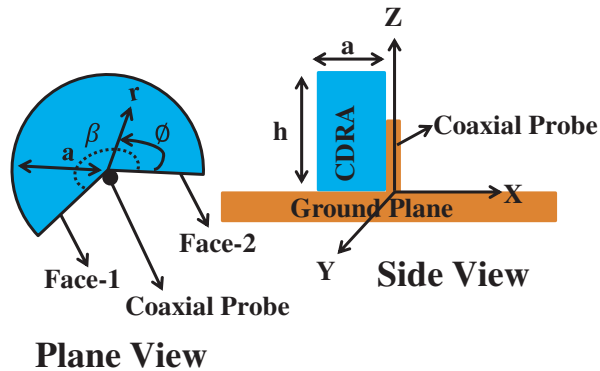
Figure 1. Geometry of cylindrical sectored DRA.

respectively, where 'm' is a positive real number, which depends upon boundary conditions, and n, p are positive integers. Due to simplicity coaxial probe feed is opted.

The half sectored cylindrical DRA (h-CDRA) is designed through splitting into two equal half of a single mold cylinder. The split is made with an arbitrary angle $\beta = \pi$ and exited with a coaxial probe at the center of the ground plane to make an h-CDRA.

The resonant frequency of the TM_{mnp} mode:

$$k_r^2 + k_z^2 = k^2 = \epsilon_r \left(\frac{2\pi f}{c} \right)^2 \tag{2}$$

where $k_r = \frac{X'_{mn}}{a}$, $k_z = \frac{(2p+1)}{2h}$ are wavenumbers.

X'_{mn} is the root satisfying $J'_m(X'_{mn}) = 0$.

So, after the modification of the equation of a half cylindrical sectored DRA, the resonant frequency calculation for the TM_{mnp} mode is [23] by the below equation

$$f_{mnp} = \frac{c}{2\pi a \sqrt{\mu_r \, \epsilon_r}} \sqrt{X'^2_{mn} + \left[\frac{\pi a}{2h} (2p+1) \right]^2} \tag{3}$$

Here μ_r is the permeability of the material, and ϵ_r is the permittivity of the material used for proposed antenna. For half cylindrical sectored DRA, $\beta = \pi$ is taken into account, and it forms single sectored CDRA face, as shown in Fig. 1. The sectored CDRA face is left open, because this approximate magnetic walls condition is observed. The magnetic walls on open faces 1 and 2 have the boundary conditions

$$\frac{\partial E_z}{\partial \phi} = 0 \text{ at } \phi = 0 \text{ and } \phi = \beta,$$

$$n = \frac{v\pi}{\beta}, \text{ where } 0 < \beta \leq 2\pi \tag{4}$$

whereas v is a nonzero positive integer to satisfy the boundary conditions for opened sectored face. The solution for opened face is required as $C = 0$. The resonant frequency depends upon diameter and height of the proposed cylindrical DRA for a particular mode.

The multi-segment (MS) h-CDRA is designed with multiple segment of different height of the h-CDRA as shown in Fig. 2. The final equation for the resonant frequency of MS h-CDRA calculating for the TM_{mnp} mode is

$$f_{mnp} = \frac{c}{2\pi a \sqrt{\mu_r \, \epsilon_{r,\text{eff}}}} \sqrt{X'^2_{mn} + \left[\frac{\pi a}{2h_{\text{eff}}} (2p+1) \right]^2} \tag{5}$$

The MS h-CDRA is formed through stacking of different dielectric materials.
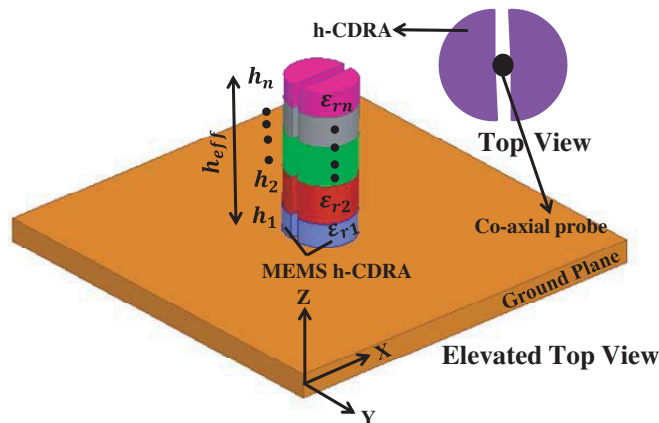
Figure 2. Geometry for formation of MEMS h-CDRA from a solid cylinder.

The effective dielectric constant ($\epsilon_{r,eff}$) and effective height (h_{eff}) can be calculated as:

$$\varepsilon_{r,eff} = \frac{h_1 + h_2 + \ldots + h_n}{h_1/_{\varepsilon_1} + h_2/_{\varepsilon_2} + \ldots + h_n/_{\varepsilon_n}} \tag{6}$$

where h_1, h_2, h_n and $\varepsilon_1, \varepsilon_2, \ldots, \varepsilon_n$ are the height and dielectric constant of the corresponding segment of the MS h-CDRA. Here $h_1 + h_2 + \ldots + h_n$ is known as effective height (h_{eff}) of the MS h-CDRA. The resonant frequency calculation of MS h-CDRA is performed through Equation (5) for $0 < \delta < 1$, and the calculated value of resonant frequency exists between 6.0 GHz and 9.5 GHz depending upon 'δ' value. Based on this multi-element multi-segment h-CDRA is designed. The two identical h-CDRAs are kept in such a way that they form a cylinder with air gap along the center axis (due to the probe at the center as a feed for coupling), as shown in Fig. 2.

The multi-element multi-segment h-CDRA (MEMS h-CDRA) is designed using splitting a mold DRA uniformly to form multi-element and stacking of that DRA with multiple layers. The DR elements are excited through coaxial probe in such a way that both elements of sectored h-CDRA touch probe at the centre, as shown in Fig. 2. For perfect matching and coupling of the h-CDRAs, the excitation is kept at the center position and for simplification of excitation; coaxial probe feed is chosen. The radius of each segment is 'a', and the effective height of MEMS h-CDRA is 'h_{eff}'. The MEMS h-CDRA has several segments (n) with every segment having its own dielectric constant ($\varepsilon_{rn}, n = 1, 2, \ldots, n$) and height ($h_n, n = 1, 2, \ldots, n$) at respective position.

Due to edge diffraction, ground plane has some effect like ripple in radiation pattern. Also due to radiation spillover, the proposed antenna reduces the gain, and due to extra current reflection, it changes the input impedance [1, 2, 27]. So, it depends upon dimension of ground plane. For minimum return loss and maximum bandwidth, the ground plane size is optimized through parametric analysis. The size of the proposed DRA is very small compare to the obtained dimension of ground plane DRA. The optimized ground plane acts as infinite ground plane for the proposed DRA. During the fabrication of the proposed prototype, a copper plate (99% copper) is used for ground plane, which is machined through a high precision lathe machine. For placing it properly adhesive material is used, and high precision Vernier scale is used for scaling. The SMA connector (50 Ω commercially available) is fitted at the center of the ground plane through screw. The h-CDRA segments are fixed by adhesive material (Fevi kwik) and also fitted with extended optimized probe. For obtaining the best antenna performance for MEMS h-CDRA, optimization of each layer with different heights is investigated.

The optimization of dual-segment (DS) h-CDRA with different layer position arrangements is tabulated in Table 1. It can be observed that due to the low dielectric constant material used below the high dielectric material is responsible for bandwidth enhancement.

The optimizations for three layers arrangement are shown in Table 2, similarly for four layers in Table 3. From Table 1, Table 2, and Table 3, it can be observed that the three segments have quite fair bandwidth and gain with easy fabrication. From Table 2 and Table 3, it can be extracted that for

Table 1. Antenna performance with segment arrangement of two elements dual segment (DS) h-CDRA (For two layers), effective height (h_{eff}) = 13 mm.

Lower Segment (I)		Upper Segment (II)		Operating Bandwidth (GHz)	Resonant Frequency (f_r) GHz	% Bandwidth	Gain (dBi)
ε_{r1}	h_1 (mm)	ε_{r2}	h_2 (mm)				
2.1	**4.0**	**9.8**	**9.0**	**5.0–11.4**	**6.5**	**98.46**	**4.85**
9.8	4.0	2.1	9.0	4.5–6.5	5.4	37.03	4.70
9.8	9.0	2.1	4.0	5.1–8.8	7.4	50.00	4.15
2.1	9.0	9.8	4.0	6.1–9.4	7.6	43.42	4.60
4.4	4.0	9.8	9.0	5.2–9.2	6.3	63.49	4.25
6.0	4.0	9.8	9.0	4.7–8.1	5.9	57.62	4.15

Table 2. Antenna performance with layer arrangement of MEMS h-CDRA (For three layers), effective height $(h_{eff}) = 13$ mm.

Lower Segment (I)		Middle Segment (II)		Upper Segment (III)		Operating Bandwidth (GHz)	Resonant Frequency (f_r) GHz	% Bandwidth	Gain at Resonant Frequency (dBi)
ε_{r1}	h_1 (mm)	ε_{r2}	h_2 (mm)	ε_{r3}	h_3 (mm)				
4.4	**3.0**	**2.1**	**5.0**	**9.8**	**5.0**	**5.4–13.4**	**6.6**	**121.2**	**6.2**
4.4	3.0	9.8	5.0	2.1	5.0	5.7–11.6	7.8	75.64	5.1
9.8	5.0	2.1	5.0	4.4	3.0	5.5–10.3	6.5	73.84	5.2
9.8	5.0	4.4	3.0	2.1	5.0	5.9–11.4	8.1	67.90	7.3
2.1	5.0	4.4	3.0	9.8	5.0	6.0–11.1	7.9	64.55	7.2
2.1	5.0	9.8	5.0	4.4	3.0	5.3–10.0	7.1	66.19	6.5
6	4.0	9.8	4.0	2.1	5.0	5.1–10.5	6.8	79.41	4.6
6	4.0	2.1	5.0	9.8	4.0	5.0–12.3	6.2	117.74	4.1
9.8	4.0	2.1	5.0	6	4.0	5.1–9.1	5.8	68.96	4.2
9.8	4.0	6.0	5.0	2.1	4.0	5.2–9.4	7.7	54.54	4.4
9.8	4.0	6.0	4.0	2.1	5.0	5.3–9.7	7.8	56.41	4.5
2.1	5.0	6.0	4.0	9.8	4.0	5.7–10.6	7.9	62.02	5.1

Table 3. Antenna performance with layer arrangement of MEMS h-CDRA (for four layers), effective height $(h_{eff}) = 13$ mm.

Segment (I)		Segment (II)		Segment (III)		Segment (IV)		Operating Bandwidth (GHz)	Resonant Frequency (f_r) GHz	% Bandwidth	Gain at Resonant Frequency (dBi)
ε_{r1}	h_1 (mm)	ε_{r2}	h_2 (mm)	ε_{r3}	h_3 (mm)	ε_{r4}	h_4 (mm)				
6.0	**4.0**	**2.1**	**3.5**	**4.4**	**1.5**	**9.8**	**4.0**	**5.2–12.5**	**5.9**	**123.73**	**5.0**
6.0	4.0	2.1	3.5	9.8	4.0	4.4	1.5	5.1–11.2	6.0	101.67	4.8
6.0	4.0	9.8	4.0	4.4	1.5	2.1	3.5	5.4–9.1	6.9	53.62	5.3
9.8	4.0	6.0	4.0	4.4	1.5	2.1	3.5	5.2–9.2	7.5	53.33	5.7
9.8	4.0	4.4	1.5	6.0	4.0	2.1	3.5	5.1–9.1	6.9	57.97	5.2
9.8	4.0	2.1	3.5	4.4	1.5	6.0	4.0	5.3–10.2	7.3	67.12	5.2
2.1	3.5	6.0	4.0	4.4	1.5	9.8	4.0	5.4–10.1	7.5	62.67	5.7
2.1	3.5	4.4	1.5	6.0	4.0	9.8	4.0	5.5–11. 4	8.2	71.95	6.2
2.1	3.5	9.8	4.0	4.4	1.5	6.0	4.0	5.7–12.3	8.4	78.57	6.3
4.4	1.5	6	4	2.1	3.5	9.8	4	5.5–12.6	8.1	87.65	6.2
4.4	1.5	2.1	3.5	6.0	4.0	9.8	4.0	5.4–12.5	8.2	86.58	6.1
4.4	1.5	9.8	4	2.1	3.5	6	4	5.3–11.5	7.3	84.93	5.2

the bandwidth enhancement, low dielectric material should be kept at the middle position to decrease its effective dielectric constant, and for proper coupling, moderate dielectric constant should be kept at lower segment near the ground plane. The highest dielectric constant material DR among them should be on the upper segment which results in high gain as well as good radiation.

The two-element three-segment h-CDRA is given a generalized name as MEMS h-CDRA, and it is fabricated for experimental investigation. The fabricated MEMS h-CDRA is shown in Fig. 4(b). For four-layer arrangement fabrication complication has to be face along with one extra segment dielectric material. So, for the three-segment two-element h-CDRA (proposed antenna), each layer height is optimized and listed in Table 4, Table 5, and Table 6.

Table 4. Middle segment thickness variation of MEMS h-CDRA [$h_{lower} = h_{eff} - h_{middle} - h_{upper}$, $h_{upper} = 5\,\text{mm}$, $\varepsilon_{r,upper} = 9.8$ and, $\varepsilon_{r,lower} = 4.4$].

	$\varepsilon_{r,middle} = 2.1$		$\varepsilon_{r,middle} = 4.4$		$\varepsilon_{r,middle} = 6.0$	
h_{middle} (mm)	% B.W	f_r (GHz)	% B.W	f_r (GHz)	% B.W	f_r (GHz)
1	57.4	6.2	42.4	8.2	32.5	8.6
2	82.5	6.7	49.5	7.9	35.4	8.4
3	91.2	6.8	51.6	7.6	38.7	8.2
4	112.3	7.5	72.8	7.7	47.8	8.0
5	**121.2**	**6.6**	88.0	7.2	51.9	7.8

Table 5. Lower segment thickness variation of MEMS h-CDRA [$h_{middle} = h_{eff} - h_{lower} - h_{upper}$, $h_{upper} = 5\,\text{mm}$, $\varepsilon_{r,upper} = 9.8$ and, $\varepsilon_{r,middle} = 2.1$].

	$\varepsilon_{r,lower} = 4.4$		$\varepsilon_{r,lower} = 6.0$		$\varepsilon_{r,lower} = 2.1$	
h_{lower} (mm)	% B.W	f_r (GHz)	% B.W	f_r (GHz)	% B.W	f_r (GHz)
1	52.3	6.4	72.6	8.4	83.6	6.9
2	83.7	6.8	62.3	8.3	61.1	7.1
3	**121.2**	**6.6**	85.4	7.7	84.2	7.8
4	105.5	7.6	76.2	6.5	71.5	8.4
5	91.8	8.5	88.5	6.3	62.9	8.6

Table 6. Upper segment thickness variation of MEMS h-CDRA [$h_{middle} = h_{eff} - h_{lower} - h_{upper}$, $h_{lower} = 3\,\text{mm}$ (constant), $\varepsilon_{r,lower} = 4.4$ and, $\varepsilon_{r,middle} = 2.1$].

	$\varepsilon_{r,upper} = 2.1$		$\varepsilon_{r,upper} = 6.0$		$\varepsilon_{r,upper} = 9.8$	
h_{upper} (mm)	% B.W	f_r (GHz)	% B.W	f_r (GHz)	% B.W	f_r (GHz)
1	51.2	9.3	73.3	9.2	76.5	8.4
2	63.3	9.1	72.5	8.7	72.6	8.1
3	52.4	9.1	65.5	8.2	65.5	7.9
4	54.5	8.8	77.8	7.4	86.2	7.6
5	77.6	8.5	97.6	7.9	**121.2**	**6.6**

The optimization approach is used to find resonant frequency for minimum reflection coefficient. The height of the layers is optimized through extensive simulation for minimum reflection coefficient. The variation of layer thickness and dielectric constant with position of layer is analyzed and shown in Table 4, Table 5, and Table 6. The desired dimensions of the proposed antenna are achieved for the best antenna performance as follows: the lower segment height ($h_{lower} = 3\,\text{mm}$), middle segment height ($h_{middle} = 5\,\text{mm}$), and upper segment height ($h_{upper} = 5\,\text{mm}$). The probe height is optimized

for minimum reflection coefficient though extensive simulations and found to be 8.1 mm from the upper surface of ground plane.

Through the optimization, the effective height ($h_{eff} = 13$ mm) and effective radius ($r_{eff} = 4$ mm) of the cylindrical DRA are obtained. The highest bandwidth is achieved through optimization at height 13 mm and radius 4 mm. The sectored CDR elements are placed in a compact way on a conducting ground plane, which has dimension 50 mm × 50 mm × 3 mm as shown in Fig. 3 and Fig. 4 for two-element dual-segment (DS) h-CDRA and two-element three-segment h-CDRA, respectively.
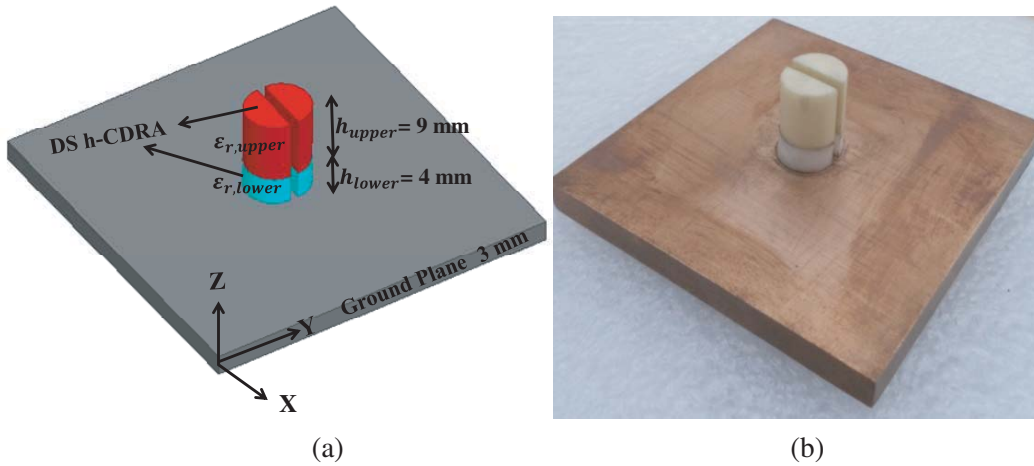
Figure 3. (a) Geometry and (b) fabricated prototype of dual segment (DS) h-CDRA.
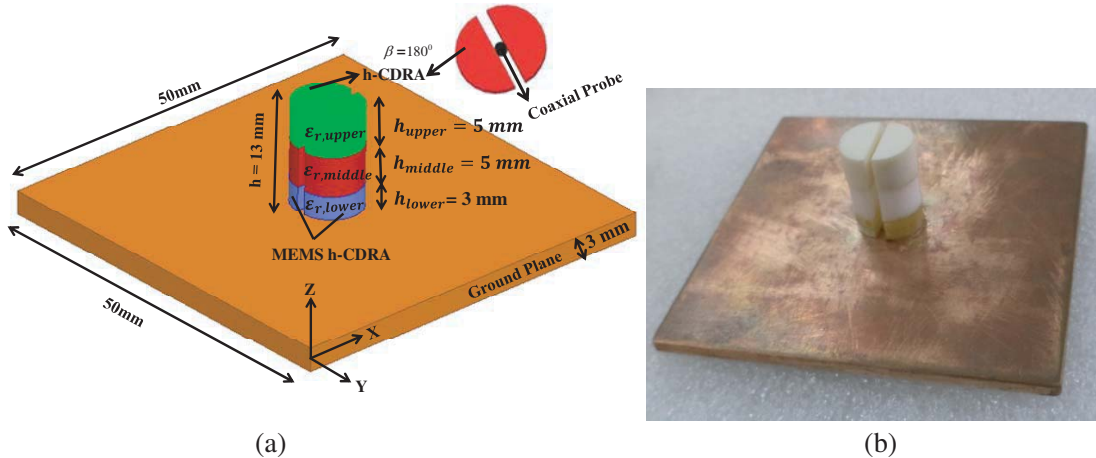
Figure 4. (a) Geometry and (b) fabricated prototype of proposed MEMS h-CDRA.

3. RESULTS AND DISCUSSION

The input characteristic of the proposed MEMS h-CDRA is studied through Ansoft HFSS simulation software. The simulated characteristics are compared with measured results. Using Rohde & Schwarz Vector Network Analyzer (Model No. ZVM, 10 MHz–20 GHz), input characteristics are measured. The measurement of far field patterns is performed inside an automatic anechoic chamber. The simulated $|S_{11}|$ vs. frequency curve of MEMS h-CDRA is compared with multi-segmented (MS) h-CDRA, which is shown in Fig. 5. The simulated $|S_{11}|$ is compared with measured one, with approximately good agreement. The simulated and measured operating frequency ranges, resonant frequencies, and percentage bandwidths of proposed MEMS h-CDRA are extracted from Fig. 5 and tabulated in Table 7.

Table 7. The performance of MEMS h-CDRA.

Parameter / Geometry	MS h-CDRA		MEMS h-CDRA	
	Simulated	Measured	Simulated	Measured
Operating frequency range ($|S_{11}| \leq -10\,\text{dB}$)	6.9–15.0 GHz	6.95–14.8 GHz	5.4–13.4 GHz	5.3–13.0 GHz
Resonant frequency	8.5 GHz	8.7 GHz	6.6 GHz	6.4 GHz
% Bandwidth	95.29%	90.22%	121.2%	120.3%
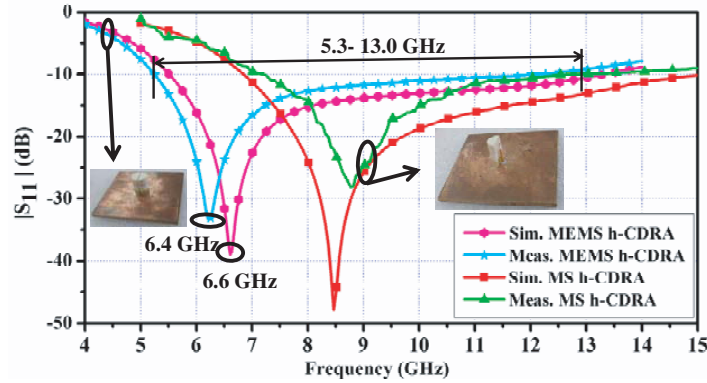
Figure 5. $|S_{11}|$ versus frequency curves of proposed MEMS h-CDRA.

Using Fig. 5 and Table 7, it can be concluded that the proposed MEMS h-CDRA provides wide bandwidth compared to MS h-CDRA. The bandwidth improvement is observed due to more effective radiation area. The wide bandwidth (120.3%) is achieved due to the low dielectric constant of the material kept below the high dielectric constant material applied to multi-segment approach.

During the fabrication, misalignment of the segment (a fabrication error) is observed as shown in Table 7. Due to the fabrication error, a slight mismatch is observed between the simulated and measured percentage bandwidths of the proposed DRA. Also, during fabrication process a small amount of glue is used to fix the h-CDRA segments, which create small difference in effective dielectric constant.

The input impedance versus frequency curve of the proposed MEMS h-CDRA is studied through Ansoft HFSS simulation, and it is compared with measured data, which is shown in Fig. 6. The measured input resistance of the proposed antenna his found to be $51.5\,\Omega$ at the resonant frequency (6.4 GHz). From Fig. 6, it can also be observed that the simulated input resistance is $48.8\,\Omega$ at the resonant frequency. The measured input resistance has close agreement with the simulated input resistance, which shows good impedance match with $50\,\Omega$ coaxial probe used for excitation.

The proposed antenna performance is compared with previously published paper, and it is listed in Table 8. It is inferred from Table 8 that the proposed antenna has better performance.

The study of simulated near field distribution of proposed MEMS h-CDRA is carried out using Ansoft HFSS simulation software at resonant frequency 6.6 GHz. The E-field and H-field distributions of the proposed MEMS h-CDRA are shown in Fig. 7(a) and Fig. 7(b), respectively. From Fig. 7(a) and Fig. 7(b) it can be observed that the proposed MEMS h-CDRA is excited with a coaxial probe, which excites $\text{TM}_{01\delta}$ as a dominant mode field in the h-CDRA element. The electric field components face their counter vectors in XY plane, which causes no radiation along the broadside direction. The resulting electric fields are polarized along Z-axis, which leads to a vertically polarized radiation pattern surrounding the radiating structure, like a quarter wave magnetic monopole [18]. On the other hand, isolated CDRA acts as an axial vertical electric dipole [4]. The proposed structure effectively produces a uniform monopole-type pattern over the full matching bandwidth at the resonance frequency.
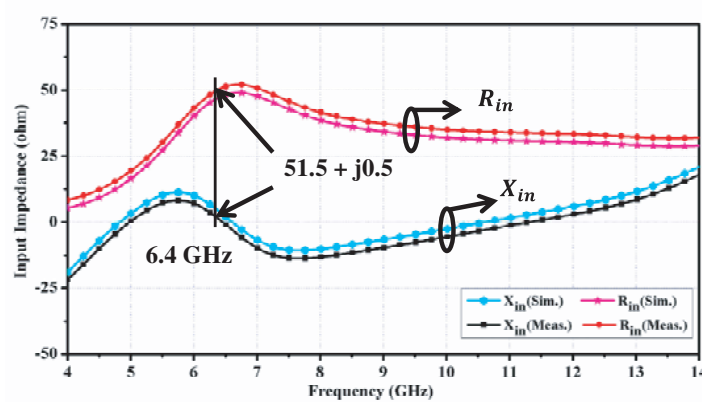
Figure 6. Variation of input impedance vs. frequency of proposed MEMS h-CDRA.

Table 8. Comparison of the proposed MEMS h-CDRA with previous published structures.

S. No.	Shape of DRA	Feeding Mechanism	Operating Bandwidth	Percentage Bandwidth ($|S_{11}| \leq -10\,\text{dB}$)	Resonant Frequency (f_r)	References
1.	Four element Cylinder	coaxial probe	3.0–4.0 GHz	29%	3.4 GHz	[10]
2.	Half split Cylinder	coaxial probe	6.6–7.6 GHz	8%	6.87 GHz	[11]
3.	Half split Cylinder	slot-coupling	7.08–7.83 GHz	10%	7.43 GHz	[12]
4.	Half split Cylinder	coaxial probe	1.7–2.3 GHz	35%	2.1 GHz	[13]
5.	Half Hemisphere	coaxial probe	2.8–4.2 GHz	35%	3.7 GHz	[14]
6.	Four element Rectangular	coaxial probe	5.0–7.0 GHz	35%	5.7 GHz	[20]
7.	Four element Triangular	coaxial probe	4.7–6.8 GHz	37%	5.45 GHz	[22]
8.	Cylindrical sector	coaxial probe	1.68–2.30 GHz	10%	1.8 GHz	[23]
9.	Half split Cylinder	coaxial probe	5.1–8.3 GHz	51%	6.25 GHz	[26]
10.	Proposed MEMS h-CDRA	coaxial probe	5.3-13.0 GHz	120%	6.4 GHz	Present Paper

The far field patterns of the proposed MEMS h-CDRA are studied through Ansoft HFSS simulation software at different frequencies in operating bandwidth. The simulated radiation patterns are compared with measurement performed in a side anechoic chamber. Inside the automatic anechoic chamber, the proposed MEMS h-CDRA his fixed through an automatic positioner as a receiver that is controlled through computer. For the source, a 2–18 GHz wideband horn antenna is placed as a transmitter antenna. The simulated and measured radiation patterns of the proposed MEMS h-CDRA in XZ, YZ, and XY planes at resonant frequency 6.4 GHz are shown in Fig. 8(a), Fig. 8(b), and Fig. 8(c), respectively. Other than resonant frequency, radiation patterns are also observed at 5.5 GHz and 9.0 GHz

(a)   (b)
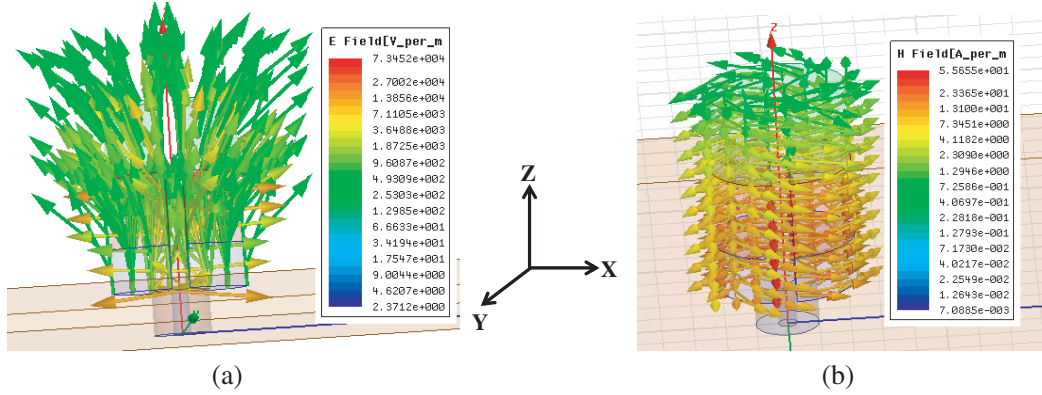
Figure 7. Near field distribution, (a) E-field and (b) H-field of proposed MEMS h-CDRA.

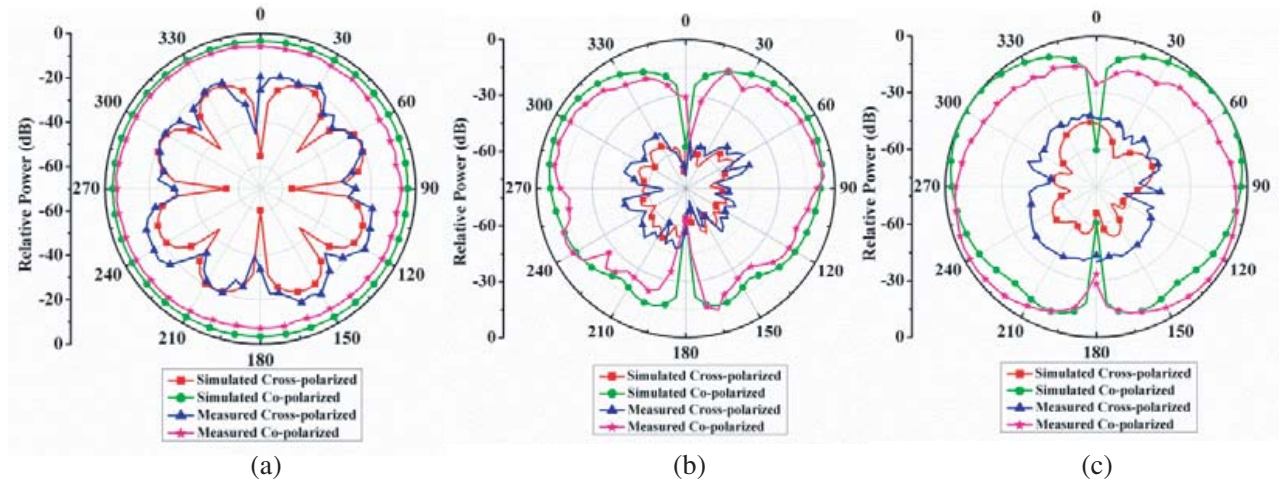(a)   (b)   (c)
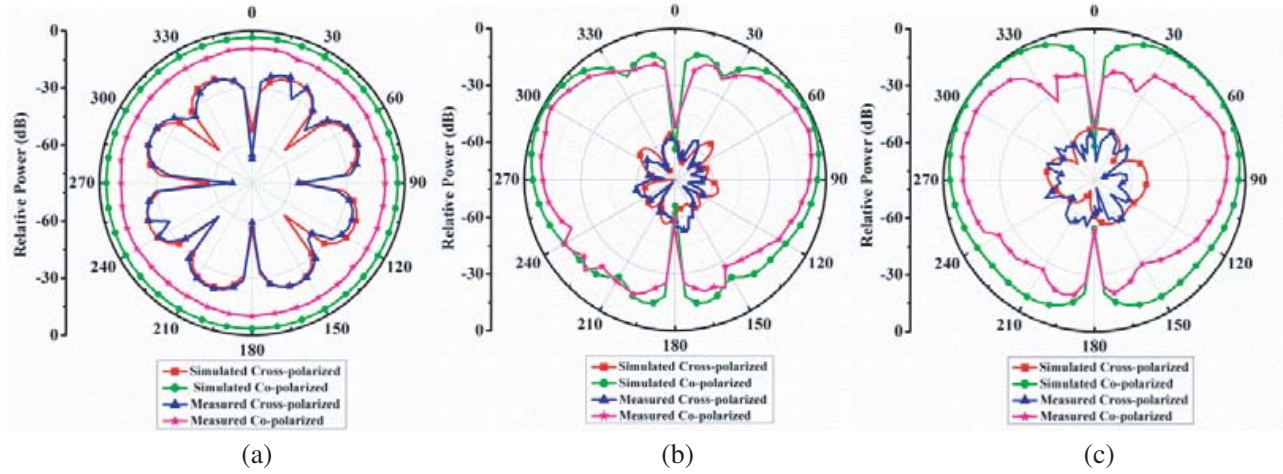
Figure 8. Radiation pattern of proposed MEMS h-CDRA (a) in XY plane, (b) in YZ plane, (c) in ZX plane at resonant frequency 6.4 GHz.

and shown in Fig. 9 and Fig. 10, respectively. The radiation pattern of the proposed MEMS h-CDRA shows omnidirectional radiation pattern in XY plane. From Figs. 8, 9, and 10, it can be observed that no radiation is along broadside direction of the proposed antenna, which confirms the offsetting E-field distributions within the elements of the proposed MEMS h-CDRA. Here it is also observed that the proposed antenna has very low cross-polarization level due to shape and height of the DRA used in protype. Fig. 8(a) shows good agreement between simulated and measured E-plane ($\phi = 0$ for XZ-plane) radiation patterns. Similarly, Fig. 8(b) shows E-plane at $\phi = 90°$ (for YZ-plane) and Fig. 8(c) shows H-plane in $\theta = 90°$ (XY-plane) radiation patterns. The simulated and measured values of co-polarization and cross-polarization levels are also in agreement for E-plane and H-plane. For the proposed MEMS h-CDRA the cross polarization level is found to be more than 30 dB down w.r.t to copolarization level in E-plane as well as H-plane. Proposed MEMS h-CDRA has monopole like radiation pattern in E-plane with null at broadside direction due to $\mathrm{TM}_{01\delta}$ mode.
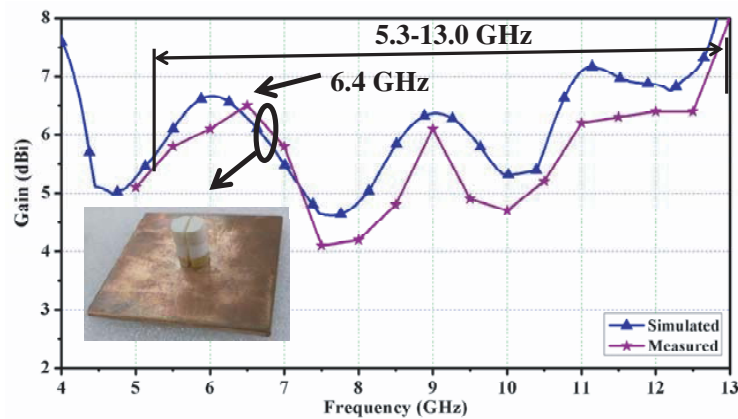
The gain vs. frequency curve of the proposed MEMS h-CDRA is shown in Fig. 11. The simulated gain is compared with measured one, and they are in close agreement with each other. Three antenna method [27] has been used for gain measurement at an tilted direction of $\theta = 60°$. From Fig. 11, it can be observed that the gain has maximum value of 6.45 dBi near resonant frequency 6.4 GHz. The gain improvement is achieved due to multi-segment approach applied on h-DRA. From Fig. 11, it can be observed that the gain is more than 4.0 dBi through the operating frequency band. Through the simulation, the value of radiation efficiency and peak directivity of the proposed MEMS h-CDRA are found 98% and 9.6 dBi, respectively.
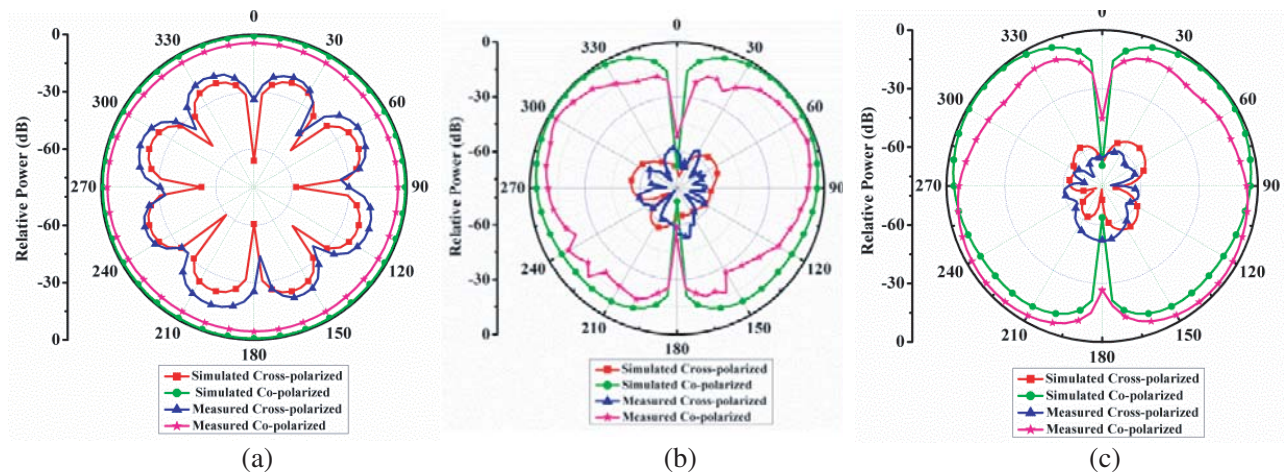
Figure 9. Radiation pattern of proposed MEMS h-CDRA (a) in XY plane, (b) in YZ plane, (c) in ZX plane at frequency 5.5 GHz.

Figure 10. Radiation pattern of proposed MEMS h-CDRA (a) in XY plane, (b) in YZ plane, (c) in ZX plane at frequency 9.0 GHz.

Figure 11. Variation of Gain vs. frequency curve of proposed MEMS h-CDRA.

4. CONCLUSION

The MEMS h-CDRA with coaxial probe feed has been designed and fabricated. The proposed MEMS h-CDRA provides wide bandwidth ($\approx 120.3\%$) with gain of 6.45 dBi at resonant frequency 6.6 GHz. The measured gain is more than 4.0 dBi in the entire operating frequency band (5.3 GHz–13.0 GHz) with a monopole type radiation pattern. The bandwidth and gain enhancement are experimentally observed. The proposed antenna has found suitable application for WLAN and WiMAX as well as X-band wireless applications.

ACKNOWLEDGMENT

REFERENCES

1. Petosa, A., *Dielectric Resonator Antenna Handbook*, Artech House, Boston, UK, 2007.
2. Kajfez, D. and P. Guillon, *Dielectric Resonator*, Artech House, Norwood, MA, 1986.
3. Long, A., A. Stuart, W. Mc. Mark, and L. C. Shen, "The resonant cylindrical dielectric cavity antenna," *IEEE Transactions on Antenna and Propagation*, Vol. 31, 406–412, 1983.
4. Mongia, R. K. and P. Bhartia, "Dielectric resonator antennas-a review and general design relations for resonant frequency and bandwidth," *Int. J. Microw. Millimeter-Wave Computer-Aided Eng.*, Vol. 4, 230–247, 1994.
5. Kishk, A. A., B. Ahn, and D. Kajfez, "Broadband stacked dielectric resonator antennas," *IET Electronics Letters*, Vol. 25, 1232–1233, 1989.
6. Petosa, A., N. Simons, R. Siushansian, A. Ittipiboon, and M. Cuhaci, "Design and analysis of multisegment dielectric resonator antennas," *IEEE Transactions on Antennas Propagation*, Vol. 48, 738–742, 2000.
7. Luk, K. M. and S. M. Shum, "Stacked annular ring dielectric resonator antenna excited by axi-symmetric coaxial probe," *IEEE Transactions on Antennas and Propagation*, Vol. 43, 889–892, 1995.
8. Gangwar, R. K., P. Ranjan, and A. Aigal, "Wideband four element two segment triangular dielectric resonator antenna with monopole-like radiation," *International Journal of Microwave and Wireless Technologies*, Vol. 9, No. 2, 411–418, 2017.
9. Saed, M. and R. Yadla, "Microstrip-fed low profile and compact dielectric resonator antennas," *Progress In Electromagnetics Research*, Vol. 56, 151–162, 2006.
10. Guha, D. and Y. M. M. Antar, "Four-element cylindrical dielectric resonator antenna for wideband monopole-like radiation," *IEEE Transaction on Antennas Propagation*, Vol. 54, 2657–2662, 2006.
11. Mongia, R. K., "Half-split dielectric resonator placed on a metallic plane for antenna applications," *Electronics Letters*, Vol. 25, 462–464, 1989.
12. Mongia, R. K., A. Ittipiboon, and Y. M. M. Antar, "A half-split cylindrical dielectric resonator antenna using slot-coupling," *IEEE Microwave and Guided Wave Letters*, Vol. 3, 38–39, 1993.
13. Kishk, A. A., A. W. Glisson, and G. P. Junker, "Bandwidth enhancement for split cylindrical dielectric resonator antennas," *Progress In Electromagnetics Research*, Vol. 33, 97–118, 2001.
14. Guha, D., B. Gupta, C. Kumar, and Y. M. M. Antar, "Segmented hemispherical DRA: New geometry characterized and investigated in multi-element composite forms for wideband antenna applications," *IEEE Transactions on Antennas and Propagation*, Vol. 60, 1605–1610, 2012.

15. Kishk, A. A., A. W. Glisson, and X. Zhang, "Analysis of a dielectric resonator antenna for wideband applications," *IEEE Transactions on Antennas and Propagation*, Vol. 50, 469–474, 2002.

16. Junker, G. P., A. A. Kishk, A. W. Glisson, and D. Kajfez, "Effect of airgap on cylindrical dielectric resonator antenna operating in $TM_{01\delta}$ mode," *Electronics Letters*, Vol. 30, 97–98, 1994.

17. Shum, S. M. and K. M. Luk, "Characteristics of dielectric ring resonator antenna with an air gap," *Electronics Letters*, Vol. 30, 277–278, 1994.

18. Mongia, R. K., A. Ittipiboon, P. Bhartia, and M. Cuhaci, "Electric monopole antenna using a dielectric ring resonator," *Electronics Letters*, Vol. 29, 1530–1531, 1993.

19. Ittipiboon, A., A. Petosa, and S. Thirakoune, "Bandwidth enhancement of a monopole using dielectric antenna resonator loading," *Proc. ANTEM Conf.*, 387–390, Montreal, Canada, 2002.

20. Lapierre, M., Y. M. M. Antar, A. Ittipiboon, and A. Petosa, "Ultra wideband monopole/dielectric resonator antenna," *IEEE Microw. Wireless Comp. Lett.*, Vol. 15, 7–9, 2005.

21. Gangwar, R. K., S. P. Singh, and D. Kumar, "Four element wideband rectangular dielectric resonator antenna terminated in bio-medium," *Wireless Personal Communications: An International Journal*, Vol. 73, 663–677, 2013.

22. Gangwar, R. K., P. Ranjan, and A. Aigal, "Four element triangular dielectric resonator antenna for wireless application," *International Journal of Microwave and Wireless Technologies*, Vol. 9, No. 1, 113–119, 2017.

23. Matthew, T. T. K. and D. R. Murch, "Compact circular sector and annular sector dielectric resonator antenna," *IEEE Transactions on Antennas and Propagation*, Vol. 47, 837–842, 1999.

24. Ranjan, P. and R. K. Gangwar, "Segmented quarter cylindrical dielectric resonator antenna: Simulation and experimental investigation in composite form for wideband applications," *International Journal of Microwave and Wireless Technologies*, Vol. 9, No. 4, 881–890, 2017.

25. Ranjan, P. and R. K.Gangwar, "Quarter cylindrical dielectric resonator antenna in multi-element composite form for wideband applications," *International Journal of Microwave and Wireless Technologies*, Vol. 9, No. 3, 639–647, 2017.

26. Ranjan, P. and R. K. Gangwar, "Probe feed half split cylindrical dielectric resonator antenna for wideband application," *AEU — International Journal of Electronics and Communications*, Vol. 69, 1709–1714, 2015.

27. Balanis, C. A., *Antenna Theory and Design*, 3rd edition, Wiley, New York, NY, USA, 2007.

28. Ranjan, P. and R. K. Gangwar, "Probe feed multi-element multi-segment triangular dielectric resonator antenna with RCS analysis," *Journal of Circuits Systems and Computers*, Vol. 28, No. 12, 1950208-1-18, 2019.

29. Ranjan, P., R. K. Gangwar, A. P. Singh, and A. Varshney, "Investigation of wideband two elements dual segment half-cylindrical dielectric resonator antenna (DS h-CDRA) with RCS analysis," *Progress In Electromagnetics Research C*, Vol. 85, 235–246, 2018.

30. Ranjan, P. and R. K. Gangwar, "Design and fabrication of high gain multi-element multi-segment quarter-sector cylindrical dielectric resonator antenna," *Frequenz. Journal of RF-Engineering and Telecommunications*, Vol. 72, Nos. 1–2, 15–25, 2018.